Materials Advances

ROYAL SOCIETY OF CHEMISTRY

REVIEW

View Article Online
View Journal | View Issue

Cite this: *Mater. Adv.*, 2022, 3, 3089

Towards improved waterproofness of Mn^{4+}-activated fluoride phosphors

Qiao Qu,† Zhaowu Wang † and Haipeng Ji *

The Mn^{4+}-activated fluoride phosphor, typically $K_2SiF_6:Mn^{4+}$, has become a renowned red-emitting phosphor for white light emitting diodes (LEDs) due to its sharp line-type luminescence spectrum peaking at ~630 nm. However, fluoride phosphors exhibit a relatively poor water resistance as $[MnF_6]^{2-}$ groups are prone to hydrolysis under humid conditions, which leads to the formation of Mn-(hydro)oxides causing a severe decrease of the luminescence efficiency. This review summarizes six strategies that have been employed to improve the waterproofness of Mn^{4+}-doped fluoride phosphors, including organic coating, inorganic heterogeneous/homogeneous coatings, surface deactivation (reduction of surface Mn^{4+}), preparation of single crystal phosphors, and other methods (solid solution, Nb^{5+} oxidation, structural rigidity-enhancement, *etc.*). The pros and cons of each strategy have been compared, and, finally, several perspectives, such as the development of single crystal phosphors with low solubility to achieve better waterproofness, have been proposed.

Received 3rd February 2022,
Accepted 2nd March 2022

DOI: 10.1039/d2ma00117a

rsc.li/materials-advances

1. Introduction

Over the last decade, white light-emitting diodes (LEDs) have found their way into many critical applications from general lighting to backlights for liquid crystal displays. For phosphor-converted white LEDs, Eu^{2+}-activated nitrides (*e.g.*, $Sr_2Si_5N_8:Eu^{2+}$, $CaAlSiN_3:Eu^{2+}$, and $Sr[LiAl_3N_4]:Eu^{2+}$), which exhibit a broad photoluminescence emission band, and Mn^{4+}-activated fluorides, which exhibit a narrower emission band (composed of multiple peaks), are the two main classes of red-emitting phosphors used in blue LED pumped white lighting.

Since the commercialization of the $K_2SiF_6:Mn^{4+}$ (KSF) phosphor by GE Global Research (USA), intense interest has been aroused on developing new Mn^{4+}-doped fluoride phosphors. KSF exhibits a broad absorption band in the blue spectral range due to the spin-allowed $^4A_2 \rightarrow {}^4T_2$ transition of Mn^{4+}, which overlaps the electroluminescence of the blue-emitting InGaN LED. It shows a series of line-type emission peaks from Stokes and anti-Stokes $\nu_6/\nu_4/\nu_3$ vibronic modes associated with Mn^{4+} $^2E \rightarrow {}^4A_2$ transition.[1,2] Each of the luminescence lines is very narrow with a full width at half maximum of <5 nm. The zero phonon line emission at 620 nm of the Mn^{4+} $^2E \rightarrow {}^4A_2$

School of Materials Science and Engineering, Zhengzhou University, Zhengzhou 450001, China. E-mail: jihp@zzu.edu.cn
† These two authors contributed equally.

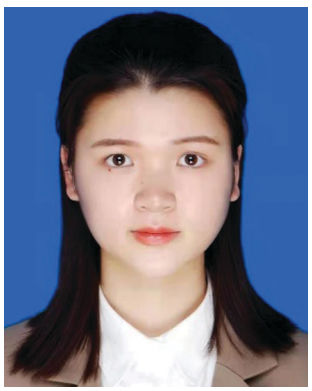

Qiao Qu

Q. Qu is now a master student at Zhengzhou University, China. Her current research focuses on Mn^{4+}-activated oxyfluoride red-emitting phosphors.

Zhaowu Wang

Z. Wang received his master's degree from the Henan University of Technology, China, in 2015. He is now a doctoral student under the supervision of Prof. Deliang Chen and Dr Haipeng Ji. His current research focuses on Mn^{4+}-activated fluoride single crystal phosphors.

transition is weak in KSF, and the Stokes ν_6 emission at 630 nm dominates the luminescence. The International Telecommunication Union proposed the use of monochromatic light at 630 nm, 532 nm and 467 nm for the red, green and blue primary colors for ultra-high definition television.[3] Since KSF exhibits luminescence of saturated red with sharp peaks, the filtering loss caused by the color filter is limited, thus benefitting the display with a wide color gamut and high color purity.

However, the main drawback of the fluoride phosphor is its sensitivity to moisture. Deterioration occurs easily due to water attack which causes the color change and lumen loss over time. This process gets accelerated when the phosphor is stressed by heat with temperatures up to ~200 °C in high brightness LEDs. Deterioration of Mn^{4+}-doped fluoride phosphors due to water attack lies in the hydrolysis of the $[MnF_6]^{2-}$ group contained in the fluoride phosphors, especially those at the surface of the particles. The dissolution of the fluoride phosphor (reaction (1); A represents alkali metal ions such as K^+, Na^+, and Cs^+, and M represents tetravalent cations such as Si^{4+}, Ge^{4+}, and Zr^{4+}) generates the $[MnF_6]^{2-}$ groups, which are prone to get hydrolysed into Mn-hydroxides and oxides,[4] possibly *via* reactions (2) and (3). The water molecule could also take the place of fluorine forming $KMnF_4{\cdot}H_2O$. This darkens the phosphor and severely weakens the intensity of red luminescence. It is thus critical to improve the waterproofness of Mn^{4+}-activated fluoride phosphors.

$$A_2M_{1-x}Mn_xF_6(s) \leftrightarrow 2A^+(aq.) + (1-x)[MF_6]^{2-}(aq.) + x[MnF_6]^{2-} \quad (1)$$

$$[MnF_6]^{2-}(aq.) + 4H_2O(l) \rightarrow Mn(OH)_4\ (s, \text{brown body color}) + 4H^+(aq.) + 6F^-(aq.) \quad (2)$$

$$Mn(OH)_4(s) \rightarrow MnO_2\ (s, \text{dark body color}) + 2H_2O(l) \quad (3)$$

Various strategies have been reported to improve the waterproofness of fluoride phosphors, which are summarized in this review. The pros and cons of each strategy were compared, and, finally, the strategy of developing single crystal phosphors with low solubility to achieve improved waterproofness was highlighted.

Haipeng Ji

Dr Haipeng Ji is an associate professor at School of Materials Science and Engineering, Zhengzhou University, China. He received his BSc and PhD degrees from the China University of Geosciences (Beijing). He has also studied in National Institute for Materials Science (Japan) and Kyoto University. He is now working in the field of inorganic photoluminescent materials.

2. Strategies to improve the waterproofness of Mn^{4+}-doped fluoride phosphors

We classify the case reported strategies to prevent the deterioration of fluoride phosphors into six classes, *i.e.*, organic coating, inorganic heterogeneous/homogeneous coating, surface deactivation, preparation of single crystal phosphors, and others.

2.1 Organic coating

Coating with hydrophobic organic compounds is a frequently used method to improve the waterproofness of fluoride phosphors. Various organic compounds have been studied to build the encapsulant layer, including alkyl phosphates, oleic acid, silane coupling agents, polypropylene glycol, *etc.*

In 2015, Nguyen *et al.*[5] reported coating the KSF particles with a 50–100 nm thick alkyl phosphate layer, obtained *via* esterification of P_2O_5 with different alcohols. The KSF particles were dispersed in an organophosphate solution of alcohols, P_2O_5, and cross-linkers. Then, the suspension was evaporated at 50–70 °C and the obtained powder was washed and heated at 150 °C for 2 h. When using Al^{3+} as the cross-linker, the phosphors exhibited an excellent moisture resistance, retaining 87% of their initial external quantum efficiency (QE) after aging under 85 °C/85% RH (RH, relative humidity) conditions for one month. In 2017, Arunkumar *et al.*[6] used oleic acid (OA) to encapsulate the KSF phosphor. OA and the phosphor were first dispersed in anhydrous ethanol, and the OA-passivated KSF (KSF-OA) was obtained by solvothermal treatment at 140 °C for 6 h. KSF-OA exhibits an internal QE of 68.1% without a decrease in the luminescence intensity compared with that of the pristine KSF. KSF-OA exhibits excellent moisture stability, retaining 85% of its initial luminescence intensity after aging for 450 h under 85 °C/85% RH conditions. The coating with OA is not detectable by X-ray diffraction (XRD) or scanning electron microscopy (SEM); only under the high-resolution transmission electron microscopy (TEM) observation, a layer with a thickness of 10 nm can be seen. As shown in Fig. 1a, the pristine KSF particles formed a brown solution after soaking in water (a phosphor concentration of 2.50×10^5 ppm) within 5 min, while KSF-OA remained unchanged after 30 min. With a phosphor concentration of 6.25×10^3 ppm and soaking in water for 15 days, the red emission of the KSF-OA sample still remained (Fig. 1b), while the emission of the pristine KSF was completely quenched. Images of the KSF and KSF-OA samples under visible and blue light excitation (λ_{ex} = 450 nm) are shown in Fig. 1c. Besides, a large increase in the ionic conductivity (28% increase, 40 mS m^{-1}) was detected for the uncoated KSF-soaked solution compared to a negligible increase in the ionic conductivity (~1% increase, 2 mS m^{-1}) for the KSF-OA case, which suggests the effective passivation effect of OA. FT-IR (Fourier transform infrared spectroscopy) and XPS (X-ray photoelectron spectroscopy) analyses indicate that hydrogen bonding (F···H) was formed between the fluorine in KSF and the hydrogen of the carboxyl group in OA (as illustrated in Fig. 1d). In addition,

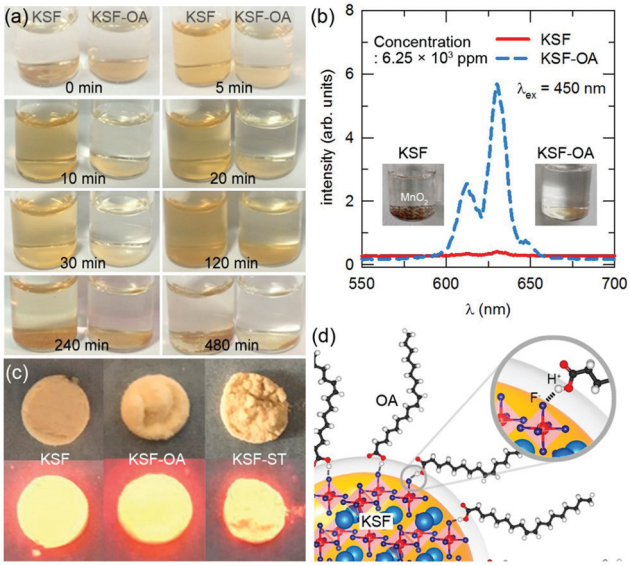

Fig. 1 Moisture stability of the KSF-OA (KSF, $K_2SiF_6:Mn^{4+}$; OA, oleic acid) phosphor. (a) Images of the pristine KSF and KSF-OA phosphors in deionized water at a concentration of 2.50×10^5 ppm for over 4 h. (b) Luminescent emission spectra of pristine KSF and KSF-OA in deionization water at a concentration of 6.25×10^3 ppm after 15 days. Inset shows the image of KSF and KSF-OA in water. A brown colored MnO_2 was formed on KSF due to the hydrolysis of MnF_6^{2-} in an aqueous medium, while the orange color is retained for KSF-OA even after 15 days. (c) Images of the pristine KSF, KSF-OA, and KSF-ST (KSF-ST is short for solvothermally treated KSF but without OA) phosphors under visible light (top layer) and blue light excitation (bottom layer). (d) Schematic of the hydrogen bonding between KSF and OA in the KSF-OA phosphor. The core elements, namely K, Si, and F, from the KSF phosphor and shell elements (C, O, and H) of the OA encapsulant are represented as pale blue, red, royal blue, gray, red, and white spheres, respectively. Reprinted with permission from ref. 6 Copyright 2017 American Chemical Society.

the bending configuration of the alkyl chain of the *cis*-form of OA ensures the complete encapsulation of KSF particles with a hydrophobic passivated skin.

In 2017, Kim *et al.*[7] modified KSF with a silane coupling agent through the dry-type plasma-assisted method. The KSF powder was pre-treated with plasma to introduce hydroxyl (–OH) groups as chemical binding sites, and, then, it was modified with silanes that have different carbon chain lengths. The water contact angle of KSF increased from 6.64° to 71.92°, 79.04° and 122.47°, respectively, which indicates that the water-resistance was reinforced as the carbon chain length of silane increased. Besides, the modified KSF exhibited enhanced light absorption and quantum efficiency due to the formation of SiO_2 coating and elimination of quenching sites. In 2018, Zhou *et al.*[8] also used silane coupling agents to coat $K_2TiF_6:Mn^{4+}$ at room temperature. The $K_2TiF_6:Mn^{4+}$ powder was first processed using an ultraviolet lamp to increase hydroxyl (–OH) groups as chemical binding sites and then mixed vigorously with silane coupling agents with different lengths of alkyl chains. The water contact angle of the modified $K_2TiF_6:Mn^{4+}$ dramatically increased from nearly 0° to 36.8°, 52.7°, 147.9°, or 155.4° after modification. The moisture resistance of the modified $K_2TiF_6:Mn^{4+}$ was much better than that of the pristine $K_2TiF_6:Mn^{4+}$, and the luminescence attenuated more slowly when the carbon chain of silane is longer.

In 2020, Hong *et al.*[9] used polypropylene glycol (PPG) to coat $BaGeF_6:Mn^{4+}$. The PPG-coated $BaGeF_6:Mn^{4+}$ was prepared *via* co-precipitation during which PPG, together with GeO_2, K_2MnF_6 and BaF_2, were added into the HF solution. The luminescence intensity of the PPG-coated $BaGeF_6:Mn^{4+}$ was 11% higher than that of $BaGeF_6:Mn^{4+}$, which can be explained by the modification of the surface defects of $BaGeF_6:Mn^{4+}$ by PPG coating. After soaking in water for 120 h, the luminescence intensity of $BaGeF_6:Mn^{4+}$ decreased by 85%, while that of $BaGeF_6:Mn^{4+}$@PPG decreased by only 65%.

In 2020, Liu *et al.*[10] used the chemical vapor deposition method to decompose acetylene on the $K_2SiF_6:Mn^{4+}$ phosphor at high temperatures. The generated nanoscale amorphous carbon layer worked as a hydrophobic protective coating. $K_2SiF_6:Mn^{4+}$@C retained 73% of the initial luminescence intensity after soaking in water for 8 h, while the pristine $K_2SiF_6:Mn^{4+}$ retained only 0.7% of the initial value.

It is seen from the above literature references that organic encapsulation can greatly improve the hydrophobicity and waterproofness of fluoride phosphors. The organic molecules could form hydrogen bonding with fluorine of the fluoride phosphor for enhanced adhesion. Generally, high temperature treatment or pretreatment to introduce binding sites is necessary for effective organic coating.

2.2 Inorganic heterogeneous coating

Various kinds of inorganic compounds, mainly metal oxides and metal fluorides, have also been used as coating materials for fluoride phosphors. Examples hereof are SiO_2, Al_2O_3, TiO_2, CaF_2, and SrF_2.

In 2019, Quan *et al.*[11] coated $KSF:Mn^{4+}$ with SiO_2 (40–80 nm thick) *via* a sol–gel process. The phosphor was dispersed in a mixture of isopropanol, tetraethyl orthosilicate (TEOS) and oleic acid. After stirring, the mixture was rinsed with isopropanol and dried at 70 °C. The prepared $KSF:Mn^{4+}$@SiO_2 exhibited high thermal stability and excellent waterproof properties with a relative luminescence intensity of ~65% after soaking for 1 h in water. In 2019, ten Kate *et al.*[12] reported coating $KSF:Mn^{4+}$ with a thin Al_2O_3 layer (3–25 nm) by atomic layer deposition (ALD) in a fluidized bed reactor. This ALD coating method is a gas-phase deposition technique based on self-limiting reactions. A layer-by-layer growth of the coating in the ALD process enables the precise control of the layer thickness by controlling the number of cycles. The coated product had a good water resistance and luminescence thermal stability. However, the use of water or ozone as the oxygen precursor during ALD caused degradation of the surface layer of $KSF:Mn^{4+}$ particles. Hence, the ALD coating with Al_2O_3 is beneficial for waterproofness not to a conventional $KSF:Mn^{4+}$ phosphor, but to a $KSF:Mn^{4+}$ phosphor with a Mn-free shell. Besides, Smet *et al.*[13] deposited Al_2O_3 or TiO_2 on the surface of the $KSF:Mn^{4+}$ phosphor also by the means of ALD. Fig. 2 shows the SEM-EDS (SEM, scanning electron microscopy; EDS, energy dispersive

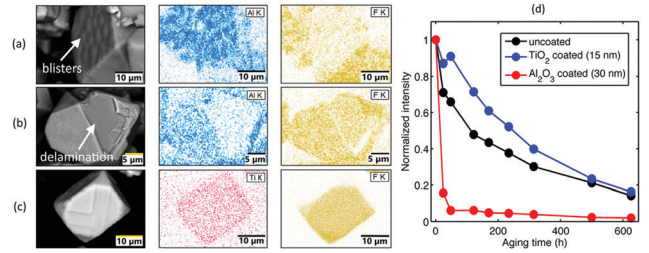

Fig. 2 SEM-EDS images of the as-deposited radiofrequency plasma enhanced-ALD-deposited K_2SiF_6:Mn^{4+}–Al_2O_3 showing (a) blistering and (b) delamination of the Al_2O_3 film. (c) SEM-EDS images of the thermal enhanced-ALD-deposited K_2SiF_6:Mn^{4+}–TiO_2. (d) Integrated phosphor emission for uncoated, Al_2O_3 or TiO_2-coated phosphors as a function of aging time in 85 °C/85% RH. Reprinted with permission from ref. 13 Copyright 2019 American Chemical Society.

spectrometry) images of the Al_2O_3 or TiO_2 deposited KSF:Mn^{4+}. The Al_2O_3 layer suffered from delamination and blistering after deposition (Fig. 2a and b) due to incompatible chemistry between the KSF:Mn^{4+} core and the Al_2O_3 shell, while the TiO_2 layer (with a thickness of ~100 nm as observed by scanning transmission electron microscopy) could be grown with a high uniformity and conformality (Fig. 2c). A probable explanation[13] of the observed delamination and blistering is the formation of volatile etch products such as $AlF_x(CH_3)_{3-x}$ by the interaction of trimethylaluminum molecules (precursors) with the fluoride substrate. Consequently, the aging test showed an enhanced stability for TiO_2-coated KSF:Mn^{4+} compared with that for the pristine powder, whereas the Al_2O_3-coated particles showed an opposite trend (Fig. 2d) with a strong brown discoloration during aging due to the MnO_2 formation.

In 2019, Dong *et al.*[14] coated K_2TiF_6:Mn^{4+} (KTF) with CaF_2. The CaF_2 solution was added to a solution of K_2TiF_6/K_2MnF_6/HF, and the mixed solution was dried at 70 °C to obtain CaF_2-coated KTF:Mn^{4+}. After soaking in an ethanol–water (2 : 3 by mass) solution, KTF dissolved immediately, accompanied by attenuation of the luminescence intensity, while KTF@CaF_2 still emitted the bright red light after 150 min. Later, in 2021, Yu *et al.*[15] coated KSF:Mn^{4+} with CaF_2 by slowly adding a $Ca(NO_3)_2$ solution into the KSF:Mn^{4+}/HF solution. After soaking in water for 6 h, the luminescence intensity of K_2SiF_6:0.055Mn^{4+} decreased to 41.68% of the initial one, while that of K_2SiF_6:0.055Mn^{4+}@CaF_2 (20 wt%) were retained 88.24% of the initial one. Similarly, Fang *et al.*[16] coated KSF:Mn^{4+} with SrF_2 by adding a $Sr(NO_3)_2$ solution to a K_2TiF_6:Mn^{4+}/KHF_2 solution. The luminescence intensities of KTF:Mn^{4+}@$xSrF_2$ (x = 0, 0.2, 0.4, 0.6, and 0.8) phosphors were still retained over 90% of initial values after soaking in water for 2 h.

The coating with metal fluorides or oxides does not guarantee a hydrophobic shell like an organic coating does. For instance, the ALD-deposited Al_2O_3 or TiO_2 shells are hydrophilic because of the presence of hydroxyl groups at the surface. Thus, the closure of the inorganic shell is critical for the improvement of waterproofness. To take advantage of the hydrophobic nature of organic coating, there are also some reports on integrated surface modification, for instance, using double-shell coatings of oleic acid and SiO_2.[17] Concerning the formation of a coating layer of inorganic metal fluorides, it is noted that high temperature treatment is not necessary.

2.3 Inorganic homogeneous coating

As early as in 2011, a patented approach was reported by Setlur *et al.*[18] to improve the moisture stability of KSF:Mn^{4+} through surface encapsulation with a Mn^{4+}-free K_2SiF_6 layer, which was obtained by treating KSF:Mn^{4+} with a mixture solution of K_2SiF_6/HF/H_2SiF_6. We call this method to obtain, for instance, KSF:Mn^{4+}@KSF, as the homogeneous coating. This is different from the heterogeneous coating since this coating layer has absolutely the same physicochemical properties (such as the refractive index and lattice constants) as the inner phosphor. Besides, the homogeneous coating may decrease the non-radiative decay probability at the surface, enhancing the luminescence intensity.

In 2019, Jiang *et al.*[19] reported a K_2SiF_6 shell on the KSF:Mn^{4+} surface obtained by ethanol-induced deposition. KSF:Mn^{4+}@KSF underwent almost no color change after soaking in water for 4 h, while KSF:Mn^{4+} turned quickly from yellow to light brown within 5 min. KSF:Mn^{4+}@KSF retained 82% of the initial luminescence intensity after being soaked in water for 4 h, and retained 90% after being exposed under 85 °C/85% RH conditions for 10 days. In the same year, Huang *et al.*[20] used a reverse cation exchange strategy to prepare the core–shell structured K_2TiF_6:Mn^{4+}@K_2TiF_6. KTF:Mn^{4+} was added to a HF solution saturated with KTF crystals, and, then, the mixture was stirred for 20 min followed by vacuum filtration. KTF:Mn^{4+}@KTF was obtained after repeating the procedures five times. The reverse cation exchange process did not change the morphology, particle size, and crystallographic structure of the phosphors. The Mn^{4+} distribution at the surfaces of KTF:Mn^{4+} and KTF:Mn^{4+}@KTF was studied by positive secondary ion mass spectroscopy (SIMS), a technique that can analyze the chemical composition of solid surfaces at a depth of several nanometers. As seen in Fig. 3, the signal peak intensity ratios of Mn/Ti for KTF:Mn^{4+} and KTF:Mn^{4+}@KTF were calculated to be about 0.19 and 0.03, respectively. Consistently, X-ray photoelectron spectroscopy (XPS) analysis indicated that the weight percentages of Mn on the KTF:Mn^{4+} and KTF:Mn^{4+}@KTF surfaces were 0.16% and 0.09%, respectively. A concentration reduction of Mn at the shell led to improved water resistance property. As seen in Fig. 4, the yellow color of KTF:Mn^{4+} quickly became brown after soaking in water for 5 min, while KTF:Mn^{4+}@KTF retained a yellow hue even after 300 min in water. Besides, after aging under 85 °C/85% RH conditions for 480 h, the luminescence intensities of the KTF:Mn^{4+}@KTF and KTF:Mn^{4+} samples packaged in silicone retained approximately 89% and 45% of their initial values, respectively (Fig. 4f). LED2 fabricated using the phosphor blends of K_2TiF_6:Mn^{4+}@K_2TiF_6 and YAG:Ce^{3+} showed a high luminous efficacy of 162 lm W^{-1} under 60 mA drive current (Fig. 4g), which retained 89% (144 lm W^{-1}) with respect to the initial value after aging under

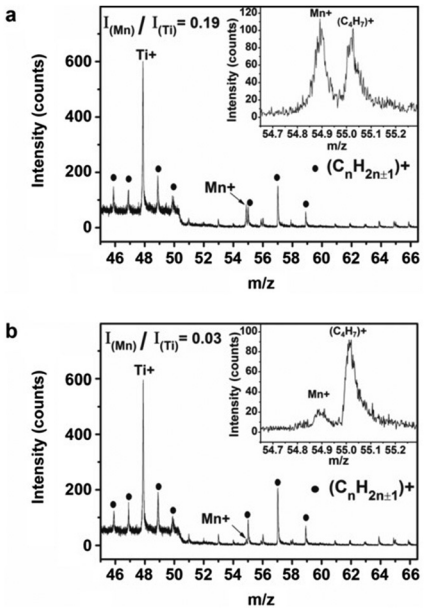

Fig. 3 Positive secondary ion mass spectra of the (a) K_2TiF_6:Mn^{4+} and (b) K_2TiF_6:Mn^{4+}@K_2TiF_6 phosphors; insets show the enlarged peak of Mn^+. Other peaks ($C_nH_{2n\pm1}^+$, solid dots) originated from the conductive tape used for fixing phosphor powders. Reprinted with permission from ref. 20 Copyright 2019 John Wiley and Sons.

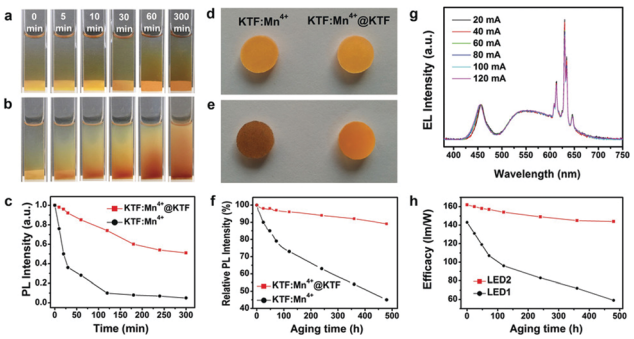

Fig. 4 Photographs of the (a) K_2TiF_6:Mn^{4+}@K_2TiF_6 and (b) K_2TiF_6:Mn^{4+} phosphors (both 0.15 g and with 7.00 at% Mn^{4+}) soaked in deionized water (3 mL) for various durations. (c) Integrated luminescence intensities of the K_2TiF_6:Mn^{4+} and K_2TiF_6:Mn^{4+}@K_2TiF_6 phosphors as a function of time in water. Photographs of the K_2TiF_6:Mn^{4+} and K_2TiF_6:Mn^{4+}@K_2TiF_6 phosphor flakes (d) before and (e) after aging under 85 °C and 85% RH conditions for 480 h. (f) Integrated luminescence intensities of the K_2TiF_6:Mn^{4+} and K_2TiF_6:Mn^{4+}@K_2TiF_6 phosphor flakes as a function of aging time. (g) Normalized electroluminescence spectra of LED2 (K_2TiF_6:Mn^{4+}@K_2TiF_6 + YAG:Ce^{3+}) under various drive currents in the range of 20–120 mA. (h) Luminous efficacies of LED1 (K_2TiF_6:Mn^{4+} + YAG:Ce^{3+}) and LED2 as a function of aging time under 60 mA drive current. Reprinted with permission from ref. 20 Copyright 2019 John Wiley and Sons.

85 °C/85% RH conditions for 480 h, demonstrating robust stability (Fig. 4h).

Later in 2021, Li *et al.*[21] reported that KSF:Mn^{4+}@KSF exhibited an improvement in both water resistance and luminescence thermal stability. The homogeneously coated phosphor was prepared by adding KSF:Mn^{4+} into the HF solution dissolved with KSF. The integrated luminescence intensity of the composite phosphor retained 88% of the initial one after soaking in water for 1 day. Meanwhile, the integrated luminescence intensities at 120, 150, 180 and 210 °C were 176, 198, 214 and 213% of the initial one at 30 °C, respectively.

The homogeneous shell is seen to not only act as a shield for preventing H_2O to hydrolyze the inner $[MnF_6]^{2-}$ group, but also cut off the energy migration path to surface defects. The formation of the inert shell is mainly obtained by soaking the phosphor into a HF solution saturated with the host compound for epitaxial growth or Mn^{4+} ion reverse exchange.

2.4 Surface deactivation

Besides homogeneous coating, the surface deactivation method was also developed to construct a Mn^{4+}-free or Mn^{4+}-rare shell. Reducing agents such as H_2O_2, DL-mandelic acid, $H_2C_2O_4$, citric acid, thiourea, glucose, phenol, and polyethylene glycol have been reported to reduce the Mn^{4+} content on the phosphor surface.

The first surface deactivation case was reported by Huang *et al.*[22] in 2018 by treating K_2SiF_6:Mn^{4+} with a H_2O_2/H_3PO_4 solution. This method generates a core–shell-like structure similar to that obtained with the homogeneous coating method, as illustrated in Fig. 5. After soaking in water (solid-to-liquid ratio of 1 g/10 mL) for 6 h, the H_2O_2-treated water-resistant phosphor (denoted as WR-KSF:Mn^{4+}) retained 76% of the initial luminescence intensity, while that of KSF:Mn^{4+} prepared by the ion exchange method (denoted as IE-KSF:Mn^{4+}) steeply decreased down to 11%. Fig. 6 shows the SEM images of the two samples before and after soaking in water for 6 h. The WR-KSF:Mn^{4+} particles show a smooth surface and a particle size of about 10 μm (Fig. 6a). After soaking in water for 6 h, there is no significant difference in micromorphology even at high magnification (Fig. 6b and c). For IE-KSF:Mn^{4+}, the original particles also showed a smooth surface (Fig. 6d), but they became more and more coarse as many nanoneedles appeared covering the surface after soaking (Fig. 6e and f). EDS analysis (Fig. 7) demonstrates that, for WR-KSF:Mn^{4+}, the content of the surface Mn ions remained almost unchanged upon soaking in water, whereas the O content at either area A or area B is below the limit of detection. In comparison, the needle-like compounds that appeared on

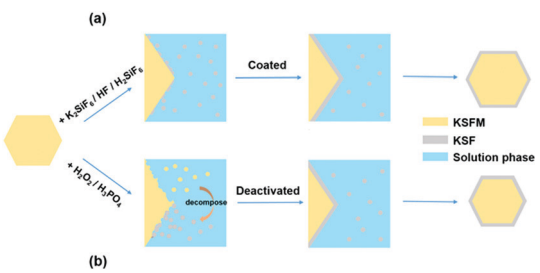

Fig. 5 Designing strategies for the K_2SiF_6:Mn^{4+}@K_2SiF_6 core–shell structure: (a) homogeneous coating and (b) surface deactivation. Reprinted with permission from ref. 22 Copyright 2018 American Chemical Society.

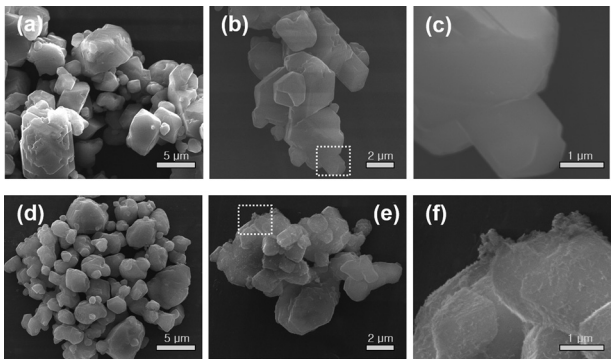

Fig. 6 SEM images of the H_2O_2-treated water-resistant K_2SiF_6:Mn^{4+}: (a) before soaking in water and (b and c) after soaking in water for 6 h, and the SEM images of K_2SiF_6:Mn^{4+} prepared *via* the ionic exchange method: (d) before soaking in water and (e and f) after soaking in water for 6 h. Reprinted with permission from ref. 22 Copyright 2018 American Chemical Society.

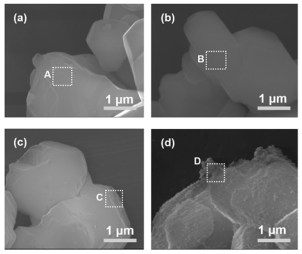

	A		B		C		D	
Element	Weight %	Atomic %	Weight %	Atomic %	Weight %	Atomic %	Weight %	Atomic %
F K	57.07 ±0.63	71.15	43.84 ±0.81	59.60	70.07 ±1.08	81.27	56.83 ±2.80	65.57
Si K	12.29 ±0.27	10.36	13.25 ±0.29	12.18	8.86 ±0.61	6.95	0.00	0.00
K K	30.19 ±0.41	18.29	42.21 ±0.45	27.88	20.46 ±0.79	11.53	16.79 ±1.14	9.41
Mn K	0.45 ±0.13	0.20	0.70 ±0.20	0.33	0.61 ±0.40	0.25	11.46 ±1.03	4.57
O K	0.00	0.00	0.00	0.00	0.00	0.00	14.92 ±2.56	20.44

Fig. 7 SEM images and EDS results of the H_2O_2-treated water-resistant K_2SiF_6:Mn^{4+}: (a, A) before soaking in water and (b, B) after soaking in water for 6 h, and the SEM images and EDS results of the K_2SiF_6:Mn^{4+} prepared *via* the ionic exchange method: (c, C) before soaking in water and (d, D) after soaking in water for 6 h. Reprinted with permission from ref. 22 Copyright 2018 American Chemical Society.

IE-KSF:Mn^{4+} after soaking do not contain any detective Si element but an excess of Mn, F, K, and especially O. Thus, the $[MnF_6]^{2-}$ group suffered a process of dissolution and hydrolysis that led to the formation of manganese (hydro)oxide. Fig. 8 shows the surface element composition of WR-KSF:Mn^{4+} as revealed by XPS. There are only K, Si, and F atoms with atomic percentages close to 2 : 1 : 6, and there is no Mn signal, indicating the formation of a KSF:Mn^{4+}@KSF core–shell

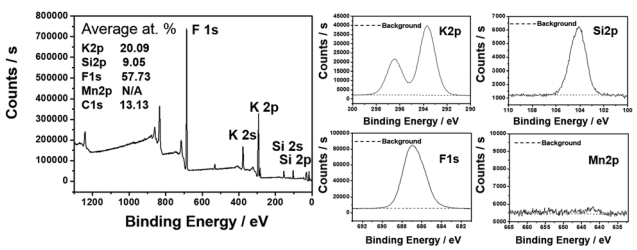

Fig. 8 X-ray photoelectron spectra (XPS) and high-resolution XPS of K 2p, Si 2p, F 1s, and Mn 2p of H_2O_2-treated water-resistant K_2SiF_6:Mn^{4+}. Reprinted with permission from ref. 22 Copyright 2018 American Chemical Society.

structure, which is responsible for excellent waterproofness properties.

In 2018, Huang *et al.*[4] used DL-mandelic acid as a reductive agent to treat K_2GeF_6:Mn^{4+}. For the pristine K_2GeF_6:Mn^{4+}, the body color quickly turned into deep brown after soaking in water for 1 h with a solid-to-liquid ratio of 1 g/10 mL, while the DL-mandelic acid-loaded K_2GeF_6:Mn^{4+} exhibited supreme moisture resistance which retained 98% of the initial luminescence intensity after soaking in water for 7 days. The improvement lies in that the surface-loaded DL-mandelic acid can *in situ* decompose Mn-oxides/hydroxides from the hydrolysate of $[MnF_6]^{2-}$ into soluble salts.

In 2019, Zhou *et al.*[23] reported the surface passivation of K_2XF_6:Mn^{4+} (X = Ti, Si, Ge) by H_2O_2 that was achieved *via* a redox reaction (reaction (4)). The surface Mn^{4+} ions of the phosphor were consumed by treating them with a H_2O_2 solution, and, then, a Mn^{4+}-rare surface was formed, which could effectively realize the isolation between the inner Mn^{4+} and the ambient moisture. Moreover, the luminescence of the H_2O-destroyed fluoride phosphors can be recovered with the addition of H_2O_2 due to the reaction between Mn^{4+}-hydrolysates and H_2O_2.

$$[MnF_6]^{2-}(aq) + 2H_2O_2(l) \rightarrow Mn^{2+}(aq) + O_2 + 2H_2O(l) \quad (4)$$

In 2019, Jiang *et al.*[24] used a $H_2C_2O_4$ reducing solution to treat Rb_2SnF_6:Mn^{4+}. The pristine Rb_2SnF_6:Mn^{4+} deteriorated rapidly after soaking in water with the body color turning brown, while the $H_2C_2O_4$-treated Rb_2SnF_6:Mn^{4+} maintained high brightness. When the concentration of the $H_2C_2O_4$ solution was 0.2 g/20 mL, the treated Rb_2SnF_6:Mn^{4+} obtained the highest luminescence intensity. Besides, compared with H_2O_2/H_3PO_4 treatment, $H_2C_2O_4$ solution treatment resulted in a better water resistance. This can be caused by the different reducibility of the solutions. The standard electrode potential of H_2O_2/O_2 (0.695 V) is higher than that of $H_2C_2O_4$/CO_2 (−0.49 V), and, thus, the reduction of Mn^{4+} in a H_2O_2/H_3PO_4 solution can be inadequate and a part of Mn^{4+} was hydrolyzed before being reduced to Mn^{2+}. Though the hydrolysis products MnO_2 or Mn^{3+} compounds can be further etched away by reduction, this caused a loosely deposited $RbSnF_6$ shell, which was easily eroded by water. Later in 2020, Yu *et al.*[25] also used a $H_2C_2O_4$ solution to treat K_2GeF_6:Mn^{4+}. The absorption efficiency and internal and external QEs of the treated phosphor were 75.7%, 62.4% and 47.3%, respectively, which are slightly lower than the values (78.4%, 70.1%, and 55.0%) for the pristine phosphor. After soaking in water (a phosphor-to-water ratio of 0.5 g/5 mL) for 5 h, the luminescence intensity of the $H_2C_2O_4$-treated K_2GeF_6:Mn^{4+} was retained at 95.8% of the initial value, while the pristine one retained only 36.2%. The formation of the Mn^{4+}-rare shell on the phosphor surface after $H_2C_2O_4$ treatment was verified by XPS and EDS analyses, which inhibited the hydrolysis of the inner $[MnF_6]^{2-}$ group. In 2020, Liu *et al.*[26] used the $H_2C_2O_4$ solution to recover the luminescence of the deteriorated K_2SiF_6:Mn^{4+} and K_2TiF_6:Mn^{4+}. The luminescence intensity of the deteriorated

$K_2SiF_6:Mn^{4+}$ or $K_2TiF_6:Mn^{4+}$ can be recovered to 103.68% or 162.59% of the original values, due to the removal of the dark-brown coating on the deteriorated phosphors and the reduction of surface defects and fine particles.

In 2021, Li *et al.*[27] used a weak reducing agent solution (citric acid or oxalic acid) to modify and/or recover the $CsNaGe_xSn_{1-x}F_6:Mn^{4+}$ phosphor. After soaking in water for 5 min, the phosphor became brown, which turned pale yellow and recovered to the initial brightness by soaking in a citric acid or an oxalic acid solution. In 2021, Jia *et al.*[28] also used citric acid and oxalic acid to modify $K_3RbGe_2F_{12}:Mn^{4+}$. A Mn^{4+}-rare shell formed on the surface of the treated phosphor, which improved the water resistance properties. Moreover, although the phosphor was quenched after soaking in water for 72 h, it got recovered to the initial brightness after soaking in the oxalic acid or citric acid solution for 2 min.

In 2021, Wan *et al.*[29] reported a reduction-assisted surface recrystallization (RSRC) strategy to construct a Mn^{4+}-free shell for $K_2SiF_6:Mn^{4+}$. To construct this Mn-free shell, when the Mn^{4+}-doped fluoride formed a saturated solution in HF reaching a dissolution–crystallization equilibrium, a reducing agent was added to the solution to remove Mn^{4+} ions, thus preventing Mn^{4+} from recrystallization. Typically, the reducing agent such as 0.4 g of TA (L-tartaric acid), 0.5 g of MA (DL-malic acid), 0.5 g of CA (citric acid), 0.1 g of AA (ascorbic acid), or 5 mL of LA (DL-lactic acid) was added to 5 mL of saturated K_2SiF_6 solution, and, then, 0.5 g of $K_2SiF_6:Mn^{4+}$ was added to the above solution under stirring for 2 h. Finally, the solids were centrifuged, washed and dried at 60 °C for 4 h. After soaking in water for 360 h, the luminescence intensity of the RSRC-treated $K_2SiF_6:Mn^{4+}$ was retained at 94% of the initial intensity, exhibiting superior waterproofness. The reducibility of TA, *etc.*, plays a key role in constructing the core–shell structure. TA is one of the α-hydroxy acids that has two carboxyl groups (–COOH) at the end and two hydroxyl groups (–OH) at the α position. The Mn^{4+} ion is considered as a strong oxidant due to its high standard electrode potential (ϕ^{Θ} = 1.64 eV) of Mn^{4+}/Mn^{2+}. In the HF solution, the hydroxyl groups of TA are easily oxidized to carbonyl groups (–CO–) and Mn^{4+} is reduced to Mn^{2+} (as illustrated in Fig. 9). The other α-hydroxy acids (lactic acid (LA), malic acid (MA) and citric acid (CA)) can also effectively eliminate Mn^{4+} on the fluoride surface in a similar manner.

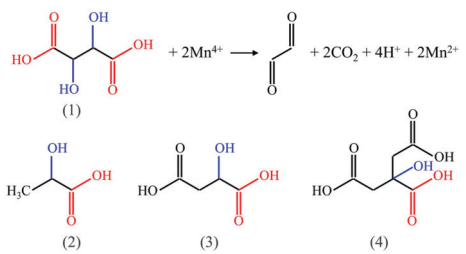

Fig. 9 Structural formulae of four α-hydroxy acids: (1) tartaric acid, (2) lactic acid, (3) malic acid, and (4) citric acid, and the possible redox reaction between the tartaric acid and Mn^{4+} ion. Reprinted with permission from ref. 29 Copyright 2021 Elsevier.

The strategy of constructing a deactivated layer with surface reduction of Mn^{4+} can evidently improve the waterproofness of fluoride phosphors. The reported reducing agents include both organic and inorganic ones with varying reducing powers. Among them, H_2O_2 will induce valence reduction not only of Mn^{4+} but also of Ti^{4+}, causing an unexpected chromogenic reaction.[23] Thus, H_2O_2 is not an appropriate surface deactivation agent for any fluotitanate phosphors. However, a drawback of the surface deactivation method is a lowered absorption efficiency due to the Mn^{4+} reduction.

2.5 Preparation of single crystal phosphors

The hydrolysis of $[MnF_6]^{2-}$ mainly occurs at the phosphor surface. Since the specific surface area of a single crystal bulk phosphor is smaller than that of the corresponding micropowder and the number of Mn^{4+} ions at the interface is less, the single crystal phosphor is better able to sustain the deterioration by water. In addition, a single crystal has fewer defects, high crystallinity, and also high thermal conductivity that facilitates the heat dissipation of LED devices. It is thus beneficial to prepare single crystal phosphors with dimensions larger than a few micrometers.

In 2016, Adachi *et al.*[30] prepared $Rb_2XF_6:Mn^{4+}$ (X = Si, Ti) single crystal phosphors (a size of ~0.5 mm) by the co-precipitation method. A mixed solution of XO_2, $RbCO_3$, $KMnO_4$ and HF was left in the dark for a few days to grow the bulk phosphors. The QE (λ_{ex} = 475 nm) reached 92% for the $Rb_2TiF_6:Mn^{4+}$ single crystal phosphor. Later, in 2018, they[31] also reported the growth of $Rb_2GeF_6:Mn^{4+}$ single crystal phosphor with a basal plane diameter of >2 mm *via* a similar co-precipitation growth method, and the QE for the bulk ingot was 87% (λ_{ex} = 475 nm).

In 2019, Wang *et al.*[32] prepared $Cs_2XF_6:Mn^{4+}$ (X = Ge, Si, Ti) single crystal phosphors (sizes of ~5 mm). Typically, 25 mmol GeO_2, H_2SiF_6 or H_2TiF_6, 60 mmol CsF and 1 mmol K_2MnF_6 were dissolved in 40 mL of HF (40 wt%) at room temperature, and the $Cs_2XF_6:Mn^{4+}$ single crystals grew from the solution after ten days. The external QEs of single crystals are as high as 66.9% (X = Ge), 63.2% (X = Si) and 52.8% (X = Ti), respectively, which are significantly higher than the data, 37.7%, 37.9%, and 32.2%, respectively, measured for the powder samples obtained by grinding the corresponding single crystals. The water resistance of single crystals is better than that of their ground powders. As shown in Fig. 10, after the $Cs_2GeF_6:Mn^{4+}$ crystal had been soaked in water for 7 h, the body color did not change obviously, and it maintained 81% of the initial luminescence intensity. On the other hand, the body color of the corresponding ground powder gradually became black, and only 9% of the initial intensity was retained after 7 h of soaking.

In 2020, Deng *et al.*[33] prepared $(NH_4)_2SiF_6:Mn^{4+}$ and $(NH_4)_3SiF_7:Mn^{4+}$ single crystals. First, undoped crystals of $(NH_4)_2SiF_6$ (sizes of 1–5 mm) and $(NH_4)_3SiF_7:Mn^{4+}$ (sizes of 3–8 mm) were grown in the saturated solutions by H_2O evaporation for over two days. Then, the NH_4HF_2 solution dissolved

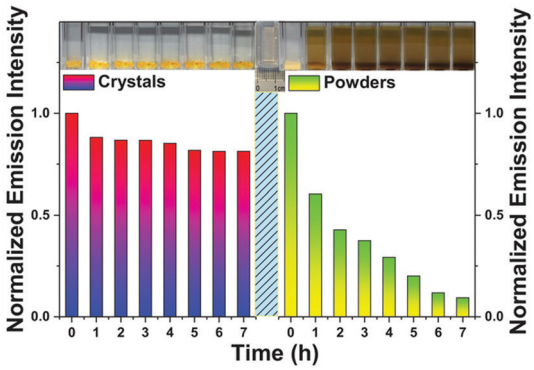

Fig. 10 Luminescence intensities of Cs_2GeF_6:Mn^{4+} crystals and powders measured after soaking in deionized water for different durations. Reprinted with permission from ref. 32 Copyright 2019 John Wiley and Sons.

with K_2MnF_6 was injected to the above crystals, and the $(NH_4)_2SiF_6$:Mn^{4+} and $(NH_4)_3SiF_7$:Mn^{4+} crystals were obtained after a fast ion-exchange within one minute. In 2021, we[34] also prepared the Na_2SiF_6:Mn^{4+} single crystal phosphor. The millimeter-sized Na_2SiF_6 single crystals with a uniform columnar morphology (2–3 mm in length) were first grown in solution by slow cooling from 90 °C to 20 °C in a water bath, which were then soaked in the HF solution dissolved with K_2MnF_6 to implement Mn^{4+} doping *via* the cation exchange process (Fig. 11a and b). Under λ_{ex} = 450 nm, the Na_2SiF_6 single crystals doped with Mn^{4+} exhibit a series of discrete sharp peaks with the intense zero phonon line emission at 617 nm (Fig. 11c and d). It was observed that, for the as-grown Na_2SiF_6 single

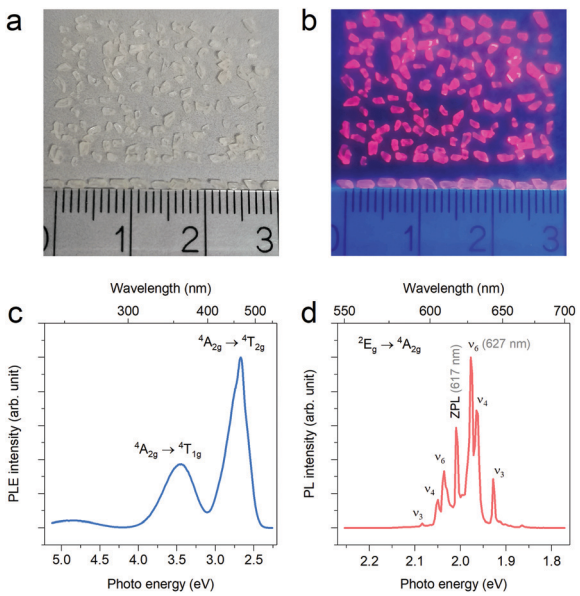

Fig. 11 Digital images of the Na_2SiF_6 crystals doped with Mn^{4+}: (a) under daylight and (b) under 365 nm ultraviolet (UV) light. The photoluminescence excitation (monitoring for 627 nm emission) and emission (under 450 nm excitation) spectra were shown in (c) and (d), respectively. Reprinted with permission from ref. 34 Copyright 2021 John Wiley and Sons.

crystals, the cation exchange reaction for Mn^{4+} doping is not effective and accompanied by by-reactions.

In 2020, Zhou *et al.*[35] grew K_2SiF_6:Mn^{4+} single crystals using a saturated crystallization method. As the growth time increased from 6 h to 4 days, the average size of the KSF:Mn^{4+} crystals increased from 200 μm to 1 mm, and, meanwhile, since $[MnF_6]^{2-}$ in the solution was gradually exhausted, the subsequent growth formed a Mn^{4+}-rare layer. The external QE of the KSF:Mn^{4+} single crystal reached as high as 78.2%, compared to 67.5% for the corresponding co-precipitated powder phosphor. Besides, after being soaked in water for 12 h, the luminescence intensity of the KSF:Mn^{4+} single crystal was retained 97.6% of the initial value, while the powder phosphor could only retain 51.8%. When the KSF:Mn^{4+} single crystal was used in white LED devices, a higher lumen efficiency and better heat dissipation were achieved.

Later, in 2021, Zhou *et al.*[36] prepared both the Cs_2TiF_6:Mn^{4+} and Cs_2TiF_6:Mn^{4+}@Cs_2TiF_6 single crystals by solvent exchange and epitaxial growth at room temperature. The maximum size of the Cs_2TiF_6:Mn^{4+} single crystal was about 11.0 mm × 3.5 mm × 1.5 mm, and the luminescence intensity was about 3.6 times that of the corresponding polycrystalline powder. The internal QE was as high as 98.7%, which is almost three times of the corresponding polycrystalline powder (30.5%). The Cs_2TiF_6:Mn^{4+} single crystal was still yellow after 48 h of aging under 85 °C/85% RH conditions, and retained almost 100% of the initial luminescence intensity, while, after aging for 6 h under 85 °C/85% RH conditions, the color of the polycrystalline powder changed rapidly from yellow to brown, and the luminescence intensity quickly decreased to 10% of the initial value. As shown in Fig. 12A, after these single crystals were soaked in water for 10 min, Cs_2TiF_6:Mn^{4+} changed from yellow to brown, while Cs_2TiF_6:Mn^{4+}@Cs_2TiF_6 remained yellow even after being soaked for 5 h. The luminescence intensity of Cs_2TiF_6:Mn^{4+} decreased monotonically with time (Fig. 12B),

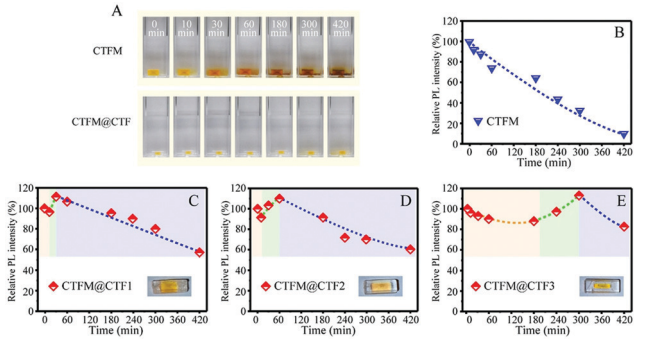

Fig. 12 (A) Photographs of Cs_2TiF_6:Mn^{4+} and Cs_2TiF_6:Mn^{4+}@Cs_2TiF_6 single crystals at different soaking periods in deionized water and integrated PL intensities of (B) Cs_2TiF_6:Mn^{4+}, (C) Cs_2TiF_6:Mn^{4+}@Cs_2TiF_6-1 (CTFM@CTF1), (D) Cs_2TiF_6:Mn^{4+}@Cs_2TiF_6-2 (CTFM2), and (E) Cs_2TiF_6:Mn^{4+}@Cs_2TiF_6-3 (CTFM@CTF3) single crystals as a function of soaking period in deionized water. The insets show the photographs of Cs_2TiF_6:Mn^{4+}@Cs_2TiF_6 single crystals with different CTF shell thicknesses: CTF1 < CTF2 < CTF3. Note: the yellow colored part is the Cs_2TiF_6:Mn^{4+} core and the colorless part is the Cs_2TiF_6 shell. Reprinted with permission from ref. 36 Copyright 2021 John Wiley and Sons.

while Cs_2TiF_6:Mn^{4+}@Cs_2TiF_6 retained a much higher luminescence intensity. This demonstrates that the core–shell structure can effectively improve the water resistance. Besides, the luminescence intensity evolution of the Cs_2TiF_6:Mn^{4+}@Cs_2TiF_6 single crystal phosphor in water exhibited a unique three-step evolution (Fig. 12C–E). The initial decrease of the luminescence intensity over time is due to the reduced transparency of the CTF shell. The following increase is due to the fact that the CTF shell has become thinner over time, which is beneficial for the light propagation from the inner CTFM core. The last decrease is in a same manner with that of Cs_2TiF_6:Mn^{4+} shown in Fig. 12B, due to deterioration of the inner Cs_2TiF_6:Mn^{4+} core.

These studies demonstrate that single crystal fluoride phosphors show superior water resistance properties compared to the powder phosphor, and a high-quality bulk ingot can be readily prepared under facile conditions due to the ionic bonding nature of fluorides. Besides, a Mn^{4+}-free shell can also be grown on the Mn^{4+}-doped single crystals for further shielding. To date, the reported maximum size of the single crystal phosphor is still around 1 mm, and the crystals are in various shapes (columns, granules, cubes, *etc.*) as the growth is restricted by the crystal structure. The applicability of these single crystal phosphors with various sizes and shapes in the all-inorganic encapsulated white LEDs needs an in-depth investigation. Moreover, the maximum Mn^{4+}-doping concentration in different compositions of fluoride single crystals is left to be unknown.

2.6 Other methods

2.6.1 Preparation of solid solution compositions. In 2020, Lang *et al.*[37] prepared K_2GeF_6:Mn^{4+} and the $K_2(Ge_{0.7}Si_{0.3})F_6$:Mn^{4+} solid solution phosphor by co-precipitation. After soaking in water, the body color of K_2GeF_6:Mn^{4+} quickly turned brown and then black, while the body color of $K_2(Ge_{0.7}Si_{0.3})F_6$:Mn^{4+} showed a slight change and the integrated luminescence intensity was retained at 78% of the initial value after 168 h. In 2020, Wang *et al.*[38] prepared $Na_2Si_{1-x}Ge_xF_6$:Mn^{4+} (x = 0, 0.5, and 1) phosphors by co-precipitation. The luminescence intensity of the x = 0.5 solid solution phosphor was retained at 71% after soaking in water for 5 h, which is twice as much as that of the Na_2SiF_6:0.06Mn^{4+} (32%) and Na_2GeF_6:0.06Mn^{4+} (33%) phosphors. The improved waterproofness of these solid solution compositions is explained by the reduction of water solubility and the enhanced Mn–F bond energy.

2.6.2 Oxidation effect of Nb^{5+} ions. In 2021, Zhou *et al.*[39] synthesized Cs_2NbOF_5:Mn^{4+} by co-precipitation, which surprisingly exhibited much better waterproofness than K_2SiF_6:Mn^{4+}. When Cs_2NbOF_5:Mn^{4+} was soaked in water, the solution became light yellow in the first 1–30 min, and then gradually turned purple over time (>60 min). The diffuse reflectance spectra indicate that this purple solution has similar absorption with the aqueous solution of $KMnO_4$. Thus, a certain amount of $[MnF_6]^{2-}$ had been oxidized to $[MnO_4]^-$ due to the disproportionation reaction occurred at the presence of Nb^{5+}. Besides, K_2NbF_7:Mn^{4+}, the as-prepared niobium-based fluoride phosphor showed a similar light yellow to purple change, which verified the oxidation of Mn^{4+} by Nb^{5+} ions. This prevented $[MnF_6]^{2-}$ from hydrolysis into brown Mn-(hydro)oxides, and thus, improved the waterproofness of fluoride phosphors.

2.6.3 Enhanced structural rigidity. In 2021, Lang *et al.*[40] improved the waterproofness of fluoride phosphors by enhancing the local structural rigidity. They used KHF_2:Mn^{4+} as the Mn source to construct a proton-containing $K_2(H)TiF_6$:Mn^{4+} phosphor. After soaking in water for 3 h, the K_2TiF_6:Mn^{4+} phosphor retained only 23% of the initial luminescence intensity, while $K_2(H)TiF_6$:Mn^{4+} retained 92% of the initial value. The reason is attributed to the fact that the proton-containing $[HMnF_6]^-$ group tends to form more rigid bonding networks and be more water resistant than the $[MnF_6]^{2-}$ group.

3. Summary and outlook

3.1 Summary

We reviewed in this paper the six classes of strategies for improving the waterproofness of fluoride phosphors, including organic coating, inorganic heterogeneous/homogeneous coating, surface deactivation, preparation of single crystal phosphors, and other methods.

For organic coating, a uniform cover with precisely controlled thickness is easy to achieve and a dramatic increase of the water contact angle after organics modification can be used as an indication of achieving waterproof properties. The coating layer should be optically transparent and evenly cover the surface of individual phosphor particles to minimize the reduction of the luminous efficacy. Besides, the complexity of the coating process, the adhesion to the phosphor particles, and the tendency of the organic layer to decompose or oxidize at high temperatures are the problems that need to be addressed.

The inorganic heterogeneous coating layer, mainly metal fluorides (CaF_2, SrF_2, *etc.*) and oxides (SiO_2, TiO_2, *etc.*), is more stable at high temperatures and have stronger adhesion. In order not to affect the luminous performance, the inorganic layer needs to be transparent in the visible range and easily coated onto the surface. However, the coating with metal oxides like Al_2O_3 is more complex and the coating process such as atomic layer deposition causes a negative effect on the fluoride phosphors. Besides, the heterogeneous coating layer can partly absorb or scatter the incoming and outgoing radiation due to the difference in the refractive index and the lattice constant between the phosphor and the shell, reducing the luminescence efficiency of the phosphor. Thus, a very thin coating layer is preferred.

Homogeneous coating is a famous patented approach which is promising to prevent fluoride phosphors from the hydrolysis reaction. A homogeneous shell also cuts down the non-radiative decay probability at the surface and enhances the luminescence intensity of the mass. Moreover, homogeneous coating can be processed using a facile wet chemical method.

Similar to homogeneous coating, surface deactivation can also generate a Mn^{4+}-rare or Mn^{4+}-free shell which shields the

inner $[MnF_6]^{2-}$ group from the hydrolysis reaction. The deactivation can be easily achieved by treating fluoride phosphors with a solution containing a reducing agent such as H_2O_2 or $H_2C_2O_4$.

The above strategies take advantage of post-treatments to enhance the waterproofness of fluoride phosphors. In comparison, the preparation of a single crystal phosphor generates bulk ingots with a lower specific surface area and less Mn^{4+} at the interface. Due to the fewer defects, the internal QE is quite often found to be higher than that of the corresponding powder phosphor. Besides, the as-grown single crystal phosphors can also be subjected to any of the aforementioned post-treatments to further enhance the waterproofness. Currently, the dominating methods for the single crystal preparation lie in the solvent volatilization and diffusion-in of poor solvents, and a new efficient method needs to be developed.

Finally, the reports employing other methods, like preparing solid solution phosphors to improve the waterproofness, are also inspiring. For example, these reports inspire to pay attention to these compositions with low solubility.

3.2 Outlook

3.2.1 Waterproofness of fluoride phosphors needs more objective assessments. Aging at a high temperature and under high humidity conditions, *i.e.*, 85 °C/85% RH, is a standard degradation evaluation process used for white LED lamps. However, there is still a lack of a standard method for the deterioration evaluation of fluoride phosphors. Typically, two methods were employed in the literature, either aging under 85 °C/85% RH conditions or soaking in water. In the first method, the effects of both the temperature and humidity on hydrolysis have been taken into consideration, and deterioration can be verified by the decrease in the luminescence intensity. The second method is conducted at room temperature and only takes the effect of humidity into consideration, but is more straightforward and easy to carry out. Using this method, deterioration can be verified not only by the decrease in the luminescence intensity (note that it can be in this case conducted in a real-time manner) but also by the physicochemical change of the solution.

The luminescence intensity measurement of a solid phosphor aggregate using a spectrometer is influenced by multiple factors, for example, the position/angle of the sample holder, the volume/packing of the phosphor, the stability of the excitation source (degradation, variation in the voltage or current), *etc.* Thus, it is a common experience that one will get a distinct luminescence intensity when measuring the same cuvette-containing phosphor aggregates twice using the same spectrometer. We recommend to measure the luminescence by placing a phosphor–water mixture-containing cuvette in an integrating sphere that is connected to a fiber optic spectrometer. Compared with a commercial spectrometer, this apparatus (illustrated in Fig. 13) is believed to get more reliable luminescence intensity by using an integrating sphere to collect the rays. Besides, as the base-located phosphor particles have contact with the cuvette and exhibit a lower hydrolysis kinetic than that of the upper surface of the phosphor aggregate which have contact with water, appropriate stirring of the phosphor suspension would help in the luminescence intensity measurement using this apparatus.

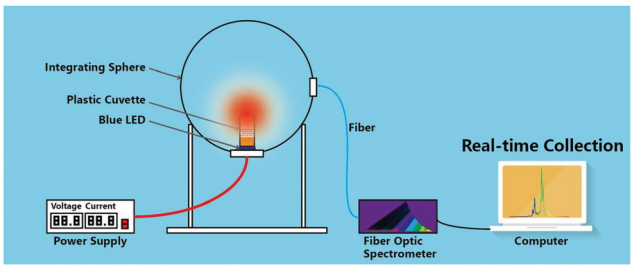

Fig. 13 Schematic of an apparatus including an integrating sphere and a fiber optic spectrometer which is recommended for use to record the photoluminescence intensity during the deterioration evaluation of Mn^{4+}-doped fluoride phosphors. Reprinted with permission from ref. 23 Copyright 2019 John Wiley and Sons.

Moreover, in addition to the luminescence intensity measurement, it is also suggested to use the QE measurement to reveal the luminescence change and the Mn valence state characterization techniques (such as X-ray photoelectric spectroscopy and diffuse reflectance spectroscopy) to reveal the hydrolysis of $[MnF_6]^{2-}$. In addition to the monitoring of the luminescence intensity, the physicochemical change of the phosphor-soaked solution, for example, the absorbance and pH (the pH usually tends to decrease due to the ionization of F^- of the fluoride phosphor), may reveal the hydrolysis of the fluoride phosphor and could be also used to evaluate the deterioration.

Finally, concerning the test method of aging in water, different phosphor-to-water ratios (often mass ratios) have been used, which makes it difficult to compare their waterproofness. As long as this aging method is widely used in the literature, it is appropriate to establish a testing standard, which, for example, sets a phosphor-to-water mass ratio for reference.

3.2.2 Preparation of singe crystal phosphors provides multiple benefits. Besides the improved waterproofness and the increase of the internal QE, the single crystal phosphor also provides an all-inorganic packaging option for white LEDs. A usual packaging approach for white LEDs is to encapsulate the powdery yellow/red phosphors onto a blue LED chip using transparent organic binders like silicone or epoxy resins. These binders are likely to experience yellowing under the attack of heat generated by the LED chip.

Fig. 14 compares the degradation of a silicone plate, a $Y_3Al_5O_{12}:Ce^{3+}$ single crystal, and a $Cs_2TiF_6:Mn^{4+}$ single crystal by thermal aging at 150 °C. The silicone was initially colorless and then turned light yellow during aging, while the body colors of the $Y_3Al_5O_{12}:Ce^{3+}$ and $Cs_2TiF_6:Mn^{4+}$ single crystals were not changed. The transmittance spectra showed that silicone had a serious decrease of transmittance and the absorption edge also showed an obvious red shift. Thus, the all-inorganic packaging free from any organic binders is a better choice, which also drives the interest of developing single crystal phosphors with suitable size.

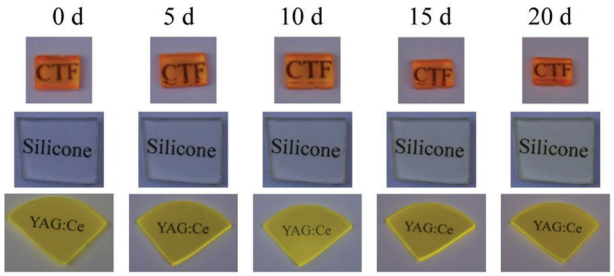

Fig. 14 Photographs of the Cs_2TiF_6:Mn^{4+} single crystal, silicone, and $Y_3Al_5O_{12}$:Ce^{3+} (YAG:Ce) crystal after heat treatment at 150 °C during different aging periods. Reprinted with permission from ref. 36 Copyright 2021 John Wiley and Sons.

3.2.3 Single crystal phosphors with low solubility would further enhance the waterproofness. To date, the reported single crystal fluoride phosphors mainly have a relatively high solubility, thus enabling the growth of single crystals from a saturated solution. As the hydrolytic degree of fluoride phosphors in water is directly related to their solubility, the more soluble the compound is, the more the ions ($[XF_6]^{2-}$, $[MnF_6]^{2-}$) generated are, and, thus, the hydrolysis reaction is promoted. For instance, the $BaSiF_6$:Mn^{4+} phosphor with a quite low solubility reported by Pan *et al.*[41] in 2016 exhibited superior waterproofness properties. The luminescence intensity of the co-precipitated $BaSiF_6$:Mn^{4+} remained almost constant after soaking in water for 30 days.

It is desired to prepare single crystal fluorides with low solubility such as alkali earth hexafluorides, which are, however, more complex. A similar solvent evaporation or diffusion-in of poor solvent treatment on a saturated solution will be encountered with a low yield problem since a saturated solution contains only a tiny amount of solute but a considerable volume of solvent. Some attempts have been recently reported. For example, the single crystal $BaTiF_6$:Mn^{4+} phosphor with a length of 200–300 μm has been prepared at room temperature by fluoridation-induced epitaxial growth.[42] More studies on the preparation of single crystal fluorides with low solubility are expected in future.

Conflicts of interest

The authors declare no conflicts of interest.

Acknowledgements

This work was supported by the Key R&D and promotion projects in Henan Province (212102210180), the Provincial and Ministerial Co-construction of Collaborative Innovation Center for Resource Materials (zycl202005), the National Natural Science Foundation of China (51902291), the China Postdoctoral Science Foundation (2019M662524), the Postdoctoral Research Sponsorship in Henan Province (19030025) and the Young Talents Lifting Project from the Henan Association for Science and Technology (2022HYTP016).

References

1 L. Helmholz and M. E. Russo, *J. Chem. Phys.*, 1973, **59**, 5455–5470.
2 A. G. Paulusz, *J. Electrochem. Soc.*, 1973, **120**, 942–947.
3 Radiocommunication Sector of ITU (ITU-R), Parameter Values for Ultra-High Definition Television Systems for Production and International Programme Exchange, 2015.
4 L. Huang, Y. Liu, S. Si, M. G. Brik, C. Wang and J. Wang, *Chem. Commun.*, 2018, **54**, 11857–11860.
5 H.-D. Nguyen, C. C. Lin and R.-S. Liu, *Angew. Chem., Int. Ed.*, 2015, **54**, 10862–10866.
6 P. Arunkumar, Y. H. Kim, H. J. Kim, S. Unithrattil and W. Bin Im, *ACS Appl. Mater. Interfaces*, 2017, **9**, 7232–7240.
7 I. Jang, J. Kim, H. Kim, W.-H. Kim, S.-W. Jeon and J.-P. Kim, *Colloids Surf., A*, 2017, **520**, 850–854.
8 Y.-Y. Zhou, E.-H. Song, T.-T. Deng and Q.-Y. Zhang, *ACS Appl. Mater. Interfaces*, 2018, **10**, 880–889.
9 F. Hong, H. Xu, G. Pang, G. Liu, X. Dong and W. Yu, *Chem. Eng. J.*, 2020, **390**, 124579.
10 Y.-X. Liu, J.-X. Hu, L.-C. Ju, C. Cai, V.-B. Hao, S.-H. Zhang, Z.-W. Zhang, X. Xu, X. Jian and L.-J. Yin, *Ceram. Int.*, 2020, **46**, 8811–8818.
11 V. T. H. Quan, D. T. Tuyet, P. J. Dereń, N. P. T. Hieu and N. H. Duy, *Vietnam J. Chem.*, 2019, **57**, 384–388.
12 O. M. ten Kate, Y. Zhao, K. M. B. Jansen, J. R. van Ommen and H. T. (Bert) Hintzen, *ECS J. Solid State Sci. Technol.*, 2019, **8**, R88–R96.
13 R. Verstraete, G. Rampelberg, H. Rijckaert, I. Van Driessche, E. Coetsee, M.-M. Duvenhage, P. F. Smet, C. Detavernier, H. Swart and D. Poelman, *Chem. Mater.*, 2019, **31**, 7192–7202.
14 Q. Dong, C. Guo, L. He, X. Lu and J. Yin, *Mater. Res. Bull.*, 2019, **115**, 98–104.
15 Y. Yu, T. Wang, X. Zhong, Y. Li, L. Wang, S. Liao, Y. Huang and J. Long, *Ceram. Int.*, 2021, **47**, 33172–33179.
16 Z. Fang, X. Lai, J. Zhang and R. Zhang, *Int. J. Appl. Ceram. Technol.*, 2021, **18**, 1106–1113.
17 M.-H. Fang, C.-S. Hsu, C. Su, W. Liu, Y.-H. Wang and R.-S. Liu, *ACS Appl. Mater. Interfaces*, 2018, **10**, 29233–29237.
18 A. A. Sultur, O. P. Siclovan, R. J. Lyons and L. S. Grigorov, *US Pat.*, 8057706B1, 2011.
19 C. Jiang, L. Li, M. G. Brik, L. Lin and M. Peng, *J. Mater. Chem. C*, 2019, **7**, 6077–6084.
20 D. Huang, H. Zhu, Z. Deng, Q. Zou, H. Lu, X. Yi, W. Guo, C. Lu and X. Chen, *Angew. Chem., Int. Ed.*, 2019, **58**, 3843–3847.
21 Y. Li, Y. Yu, X. Zhong, Y. Liu, L. Chen, S. Liao, Y. Huang and H. Zhang, *J. Lumin.*, 2021, **234**, 117968.
22 L. Huang, Y. Liu, J. Yu, Y. Zhu, F. Pan, T. Xuan, M. G. Brik, C. Wang and J. Wang, *ACS Appl. Mater. Interfaces*, 2018, **10**, 18082–18092.
23 Y. Zhou, E. Song, T. Deng, Y. Wang, Z. Xia and Q. Zhang, *Adv. Mater. Interfaces*, 2019, **6**, 1802006.
24 C. Jiang, M. G. Brik, A. M. Srivastava, L. Li and M. Peng, *J. Mater. Chem. C*, 2019, **7**, 247–255.

25 H. Yu, B. Wang, X. Bu, Y. Liu, J. Chen, Z. Huang and M. Fang, *Ceram. Int.*, 2020, **46**, 18281–18286.
26 L. Liu, D. Wu, S. He, Z. Ouyang, J. Zhang, F. Du, J. Peng, F. Yang and X. Ye, *Chem. – Asian J.*, 2020, **15**, 3326–3337.
27 D. Li, Y. Pan, X. Wei and J. Lin, *Chem. Eng. J.*, 2021, **420**, 127673.
28 Y. Jia, Y. Pan, Y. Li, L. Zhang, H. Lian and J. Lin, *Inorg. Chem.*, 2021, **60**, 231–238.
29 P. Wan, Z. Liang, P. Luo, S. Lian, W. Zhou and R.-S. Liu, *Chem. Eng. J.*, 2021, **426**, 131350.
30 S. Sakurai, T. Nakamura and S. Adachi, *ECS J. Solid State Sci. Technol.*, 2016, **5**, R206–R210.
31 S. Sakurai, T. Nakamura and S. Adachi, *Jpn. J. Appl. Phys.*, 2018, **57**, 22601.
32 Z. Wang, Z. Yang, N. Wang, Q. Zhou, J. Zhou, L. Ma, X. Wang, Y. Xu, M. G. Brik, M. D. Dramićanin and M. Wu, *Adv. Opt. Mater.*, 2019, **8**, 1901512.
33 T. Deng, E. Song, Y. Zhou, J. Chen, W. Liu, H. Deng, X. Zheng and H. Huang, *J. Alloys Compd.*, 2020, **847**, 156550.
34 Z. Wang, H. Ji, Z. Zhang, J. Xu and D. Chen, *J. Am. Ceram. Soc.*, 2021, **104**, 5077–5085.
35 Y. Zhou, C. Yu, E. Song, Y. Wang, H. Ming, Z. Xia and Q. Zhang, *Adv. Opt. Mater.*, 2020, **8**, 2000976.
36 J. Zhou, Y. Wang, Y. Chen, Y. Zhou, B. Milićević, L. Zhou, J. Yan, J. Shi, R.-S. Liu and M. Wu, *Angew. Chem., Int. Ed.*, 2021, **60**, 3940–3945.
37 T. Lang, T. Han, S. Fang, J. Wang, S. Cao, L. Peng, B. Liu, V. I. Korepanov and A. N. Yakovlev, *Chem. Eng. J.*, 2020, **380**, 122429.
38 F. Hong, G. Pang, L. Diao, Z. Fu, G. Liu, X. Dong, W. Yu and J. Wang, *Dalton Trans.*, 2020, **49**, 13805–13817.
39 J. Zhou, Y. Chen, C. Jiang, B. Milićević, M. S. Molokeev, M. G. Brik, I. A. Bobrikov, J. Yan, J. Li and M. Wu, *Chem. Eng. J.*, 2021, **405**, 126678.
40 T. Lang, J. Wang, T. Han, M. Cai, S. Fang, Y. Zhong, L. Peng, S. Cao, B. Liu, E. Polisadova, V. Korepanov and A. Yakovlev, *Inorg. Chem.*, 2021, **60**, 1832–1838.
41 Y. Pan, Z. Chen, X. Jiang, S. Huang and M. Wu, *J. Am. Ceram. Soc.*, 2016, **99**, 3008–3014.
42 Z. Wang, X. Wang, H. Ji, J. Xu, Z. Zhang and D. Chen, *Inorg. Chem.*, 2021, **60**, 13212–13221.